



LAWRENCE
LIVERMORE
NATIONAL
LABORATORY

Crystal Dynamics of (δ) fcc Pu-Ga by High Resolution Inelastic X-Ray Scattering

J. Wong, M. Krisch, D. Farber, F. Occelli, R. Xu, T. C.
Chiang, D. Clatterbuck, A. J. Schwartz, M. Wall, C.
Boro

October 29, 2004

Physical Review B

Disclaimer

This document was prepared as an account of work sponsored by an agency of the United States Government. Neither the United States Government nor the University of California nor any of their employees, makes any warranty, express or implied, or assumes any legal liability or responsibility for the accuracy, completeness, or usefulness of any information, apparatus, product, or process disclosed, or represents that its use would not infringe privately owned rights. Reference herein to any specific commercial product, process, or service by trade name, trademark, manufacturer, or otherwise, does not necessarily constitute or imply its endorsement, recommendation, or favoring by the United States Government or the University of California. The views and opinions of authors expressed herein do not necessarily state or reflect those of the United States Government or the University of California, and shall not be used for advertising or product endorsement purposes.

Crystal dynamics of fcc Pu-Ga by high resolution inelastic x-ray scattering

Joe Wong^{1,*}, M. Krisch², D. L. Farber¹, F. Occelli¹, R. Xu³, T.-C. Chiang³, D. Clatterbuck¹,

A. J. Schwartz¹, M. Wall¹, and C. Boro¹

¹*Lawrence Livermore National Laboratory, University of California, PO Box 808, Livermore, CA 94551, USA*

²*European Synchrotron Radiation Facility, BP 220, F-38043 Grenoble Cedex, France*

³*Department of Physics and Frederick Seitz Materials Research Laboratory, University of Illinois at Urbana-Champaign, 1110 West Green Street, Urbana, IL 61801, USA*

ABSTRACT

We have used a *microbeam on large grain sample* concept to carry out an inelastic x-ray scattering experiment to map the full phonon dispersion curves of an fcc δ -phase Pu-Ga alloy. This approach obviates experimental difficulties with conventional inelastic neutron scattering due to the high absorption cross section of the common ^{239}Pu isotope and the non-availability of large (mm size) single crystal materials for Pu and its alloys. A classical Born von-Kármán force constant model was used to model the experimental results, and no less than 4th nearest neighbor interactions had to be included to account for the observation. Several unusual features including, a large elastic anisotropy, a small shear elastic modulus, $(C_{11} - C_{12})/2$, a Kohn-like anomaly in the $T_1[011]$ branch, and a pronounced softening of the $T[111]$ branch towards the L point in the Brillouin are found. These features can be related to the phase transitions of plutonium and to strong coupling between the crystal structure and the $5f$ valence instabilities. Our results represent the first full phonon dispersions ever obtained for any Pu-bearing material, thus ending a 40-year quest for this fundamental data. The phonon data also provide a critical test for theoretical treatments of highly correlated $5f$ electron systems as exemplified by recent dynamical mean field theory (DMFT) calculations for δ -plutonium.

I. INTRODUCTION

Plutonium (Pu) is certainly the most astonishing of the actinides, the class of the elements in which the $5f$ electron shell is progressively filled. Indeed, in the early part of this series (Th, Pa, U and Np), the $5f$ electrons contribute to the bonding between atoms. The $5f$ participation in bonding results in an atomic volume dependence on electron population similar to that of the transition metal series. On the other hand, the heavier members of the actinide series (Am and beyond) have larger atomic volumes that are almost independent of the $5f$ electron population. This behavior resembles those of the lanthanide elements; the $5f$ states are localized and do not participate in the bonding. In Pu, the $5f$ electrons are “on the edge,”¹ and it is this unique $5f$ configuration that gives this element a host of unusual properties.² Since the discovery of Pu in 1941, the element’s eccentricities have both awed and perplexed researchers. Although the element’s complexity and unpredictability have rendered it a challenge to study, scientists persist because of the need to understand and predict plutonium’s behavior under various temperatures and pressures and to determine how the element might vary over time. Understanding its properties is indeed critical for the safe handling, use, and long-term storage of this highly toxic and radioactive material.³

The most notably unusual property of Pu is perhaps the presence of 5 solid-state allotropic phase transformations in the pure element. The α phase, which is stable from low temperature to 122°C, transforms successively to $\beta \rightarrow \gamma \rightarrow \delta \rightarrow \delta' \rightarrow \epsilon \rightarrow$ liquid with increasing temperature⁴ accompanied by large volume expansions and collapses along the way to the melt. The pure metal melts at a relatively low temperature ~640°C to yield a liquid which is higher in density than that of the solid from which it melts. The fcc (face-centered-cubic) δ phase is the equilibrium phase in the range 319 – 451°C, and has a density of 15.92g/cc. This high temperature δ phase can be stabilized or more correctly retained at room temperature and below by alloying with small amounts of Group III metals such as Al or Ga.⁵

In doing so, the metastable δ -phase field is expanded from high temperature to room temperature and below at the expense of the γ and β phases⁶, suggesting very similar ground state energies for these structures.⁷

Understanding the physical basis for the intriguing properties of Pu materials such as force constants, sound velocities, elastic constants, phase stability and thermodynamic properties critically hinges on the ability to produce high quality experimental data. Of these, phonon dispersion curves (PDCs) are key to the elucidation of many of these physical phenomena. However, PDCs in plutonium and its alloys have defied measurement for the past few decades. This is due to a combination of the high thermal-neutron absorption cross section of the most common isotope (^{239}Pu) and the inability to grow the large single crystals (with dimensions of a few millimeters) necessary for inelastic neutron scattering. These limitations have recently been overcome experimentally by the application of the high resolution inelastic x-ray scattering (HRIXS)⁸ technique combined with the use of an x-ray beam focused to microns size on large single-crystal domains in polycrystalline specimens. With this method, samples with volumes as small as 10^{-4} mm^3 can now be studied. These capabilities have opened up new experimental opportunities for materials which are only available in small quantities, as is the case for many actinide systems,⁹ and enabled us to recently map the full PDCs of an fcc δ -Pu-Ga alloy.⁸

Moreover, only recently have theoretical computations of the Pu PDCs begun to overcome the difficulties in treating the $5f$ electrons accurately within the standard first-principles methods.¹⁰⁻¹² Thus, the PDCs for Pu-bearing systems have remained essentially unknown experimentally, and theoretically until recently.

The experimental details associated with the *microbeam on large grain sample* approach in combination with the use of HRIXS to map the full PDCs of an fcc δ Pu-Ga alloy are presented in Sec.

II. The data and lattice dynamical calculations are presented in Sec. III. Section IV discusses the Born von Kármán analysis, phonon-derived elastic and thermodynamic properties, phonon softening and phase transformations, the Kohn effect and theoretical considerations. Our conclusions are summarized in Sec. V. This study provides the first full bona-fide data set for realistic calculations and simulations of thermodynamic and other physical properties for Pu and its alloys. The phonon dispersion results also provide a critical test for theoretical treatments of highly correlated $5f$ electron systems, as exemplified by recent dynamical-mean-field-theory calculations for δ -plutonium¹¹ with excellent qualitative and semi-quantitative agreement between theory and experimental data.

II. EXPERIMENTAL DETAILS

Our samples were large-grain polycrystalline specimens prepared by a strain-enhanced recrystallization technique from an fcc δ Pu-Ga alloy containing 2 at. % Ga.¹³ A cylinder of the homogenized alloy, 2.8 mm diameter by 2mm high was first uniaxially compressed by 6% and annealed at 430°C in a vacuum (5×10^{-5} Torr) for 5 days. Two such strain-anneal cycles were used. The doubly annealed cylinder was then sliced at 45 deg. to the cylinder axis into 3 slices, each $\sim 500\mu\text{m}$ thick using a low speed diamond blade ($150\mu\text{m}$ wide blade) saw. The discs were lapped with a succession of lapping films, 600 grit SiC, $30\mu\text{m}$, $12\mu\text{m}$, and $3\mu\text{m}$ $\gamma\text{-Al}_2\text{O}_3$ to a thickness of $\sim 40\mu\text{m}$. A fine polish with $1\mu\text{m}$ diamonds followed to remove $\sim 12\mu\text{m}$ from each side, yielding a thickness of $\sim 16\text{-}18\mu\text{m}$. The samples were then electropolished from both sides using a TEM (transmission electron microscopy) electropolishing system such that a shallow dimple was electrochemically removed from both side of the disc specimens to render a final thickness of $\sim 8\text{-}10\mu\text{m}$. This thickness is about one absorption length for $\delta\text{-Pu}$ ¹⁴ at 21.747 keV allowing for optimal IXS measurements in transmission geometry. This procedure produced a microstructure with an average grain size of ~ 90

μm as shown in Fig. 1. The samples were dip coated in liquid polyamide and cured at 50°C for 1 hr. This provided the first containment layer. The polyamide coated Pu-Ga foil was then loaded into a leak-proof stainless steel cell in a dry nitrogen atmosphere. The cell contains a pair of kapton windows each $125\ \mu\text{m}$ thick which provide a second level of containment. An additional metal containment was used for each sample cell for shipment from Livermore to Grenoble in accordance with the U.S. Department of Transportation regulations and the French CIREA approved procedures for handling and transporting radioactive materials.¹⁵

High resolution IXS experiments were conducted on beamline ID28 at the European Synchrotron Radiation Facility (ESRF) in Grenoble, France. The storage ring was operating at an electron energy of 6 GeV and injection current of 200 mA. The synchrotron radiation was monochromatized at 21.747 keV utilizing the Si(11 11 11) configuration to yield a total instrumental energy resolution of 1.8 meV full-width-at-half-maximum (FWHM) with the dimensions of the focused x-ray beam $30\ \mu\text{m}$ horizontal x $60\ \mu\text{m}$ vertical FWHM (see Fig. 1). With this beam, the flux on the sample was measured to be $\sim 3 \times 10^9$ photons/s. The scattered photons were energy-analyzed by five crystal analyzers in Rowland circle geometry employing the same reflection order as the high-resolution backscattering monochromator. The momentum transfer, $Q = 2k_0\sin(\theta_s/2)$, where k_0 is the wave vector of the incident photons and θ_s the scattering angle, was selected by rotating the spectrometer arm in the horizontal plane. The momentum resolution was set by slits to $0.4\ \text{nm}^{-1}$. An on-line fluorescent screen, coupled to a CCD camera, allowed us to map and select single-crystal domains in the specimen, and orient them according to the requirements of the scattering geometry for the longitudinal and transverse acoustic phonon branches. With the small beam dimensions, single-crystal domains could be selected with a typical mosaic spread ranging between 0.5 and 1.5 degrees. In

the longitudinal geometry, after appropriate momentum transfer corrections,¹⁶ the spectra of all five analyzers could be utilized. This was not possible for the transverse scans, and therefore the spectrum of only one analyzer was utilized. The energy scans were performed by varying the monochromator temperature while the analyzer temperature was kept constant. Conversion from the temperature scale to the energy scale is accomplished by using the following relation: $\Delta E/E = \alpha \Delta T$, where $\alpha = 2.58 \times 10^{-6} \text{ K}^{-1}$ is the linear thermal expansion coefficient of Si at room temperature. Details of the HRIXS instrumentation have been described elsewhere.¹⁷ All phonon spectra in this study were collected at room temperature.

III. RESULTS

Typical IXS spectra (Fig. 2) are shown for longitudinal acoustic (LA) phonons along the [111] direction at selected reduced momentum transfer values ($\xi\xi\xi$). At a given q value, the count rate with error bars is plotted versus the energy of the analyzer. Each spectrum in Fig. 2 results from a sum of two individual 4-hr scans. For each scan, the integration time per data point was 90s. The spectra are each characterized by an elastic contribution centered at zero energy and two inelastic contributions, corresponding to the creation (energy-loss, Stokes) and annihilation (energy gain, anti-Stokes) of an acoustic phonon. In order to extract the phonon energies, the spectra were fitted by using a standard χ^2 minimization procedure constraining the system by assuming an equal energy separation of the Stokes and anti-Stokes excitations from the central Rayleigh line with the intensity ratio governed by the thermal phonon population factor, and by convolving the experimental spectra with three model Lorentzian functions to match the intrinsic energy resolution profiles of the instrument.

Values of the phonon energies for the three principal directions of the fcc δ Pu-Ga fcc structure, with estimates of overall errors resulting from the χ^2 minimization algorithm, are given in Table 1. The

experimental phonon dispersion curves along the three symmetric directions are plotted as points in Fig. 3, together with a fit (colored lines) obtained by means of a standard Born-von Kármán (B-vK) force constant model.¹⁸ An adequate fit to the experimental dispersions is obtained with this method if interactions up to the fourth nearest neighbor are included. Along the $[\xi 00]$ and $[\xi \xi \xi]$ directions, the transverse modes are degenerate and z , the direction of vibration of the single atom in the unit cell, may lie in any direction normal to \mathbf{q} . Along the $[\xi \xi 0]$ direction, the two transverse modes are distinct with z lying in the $[01\bar{1}]$ and $[001]$ directions for T_1 and T_2 respectively.

Three unusual features in the PDCs of δ Pu-Ga alloy are noteworthy: (a) similarity in the slopes of the $LA(\xi 00)$ and $TA(\xi 00)$ branches, (b) a kink in the $T_1(\xi \xi 0)$ indicative of a Kohn anomaly¹⁹ and (c) a pronounced softening of the $TA(\xi \xi \xi)$ branch towards the L point. These features will be discussed in detail below.

IV. DISCUSSION

1. Born-von Kármán Analysis

The experimental dispersion curves can be analyzed using the classical Born-von Kármán (B-vK) model with various coordination shells of interacting neighbors. Using a procedure of linear least squares fitting to the dispersions, inter-atomic force constants as well as inter-planar force constants are determined.²⁰ In a fcc lattice there is insufficient information in the dispersion curves along the principal symmetry directions to permit a fit beyond the fourth nearest neighbors (4NN). Constraints on the long-range force constants must be imposed to include higher neighbors. For example, two axially symmetric constraints are needed for a six nearest neighbor (6NN) model and four for an eight-nearest neighbor (8NN) model (see Table 2).

A series of B-vK calculations has been performed systematically using models with 2NN to 8NN to fit the IXS data. The inter-atomic force constants obtained from these models are listed in Table 2. As seen in Fig. 3 (colored lines), when no constraints are imposed and the forces extending to 4NN are considered, a reasonable fit to the dispersion curves is obtained. In Fig. 4, the goodness of fit, χ^2 , is plotted versus the number of neighbors included in the fit. At 3NN, χ^2 drops significantly but decreases much more slowly upon including additional neighbors. In fact, beyond 4NN, the long-range force constants turn out to be much smaller. Extending the fit to eighth neighbors improves the goodness of the fit somehow, but the fits tend to reproduce the noise wiggles and unphysical oscillations.

As noted by Dutton et al.,²¹ in the fcc lattice, fourth neighbors are the most distant which can be reached in two *nearest-neighbor* steps. From this structural consideration it seems reasonable that the force constants for neighbors more distant than fourth have distinctly smaller values. Furthermore, it is interesting to note that the 4NN model for a fcc lattice includes a total of 54 atoms about a central atom: 12 (110)-neighbors from the first coordination shell, 6 (200)-neighbors from the second shell, 24 (211)-neighbors from the third and 12 (220)-neighbors from the fourth shell. By composition, the 54 neighbors contain a Ga atom in the Pu-2 at. % Ga alloy, implying that the Ga has to be included in the crystal dynamics of the system within the B-vK framework.

2. Elastic Properties

The sound velocity, V , associated with each of the phonon branches shown in Fig. 3 can be determined directly from a linear fit to the low q region around the Γ point and are shown in Table 3. The elastic moduli, C_{ij} , are then computed directly using $C_{ij} = \rho \cdot V^2$, where ρ is the density of the Pu-Ga alloy and equals 15.82 gm/cc at room temperature. In a cubic crystal, if the interatomic forces are

central (ie.: purely radial, angle independent), then the Cauchy relation for the second order elastic constants is fulfilled.²²

$$C_{44} = C_{12}.$$

Deviations from this relation account for the existence of non-central forces. In Table 4, the experimental elastic constants of all fcc metals reported in the literature²³⁻⁴³ are listed. Most of these elastic moduli were determined from inelastic neutron scattering, except for those of Ir²⁴, Pt²⁵, Rh²⁶ and Th³⁶, which were determined from ultrasonic measurements. The elastic constants for Pt were measured at 90K²⁵, and those of β -La²⁷ and γ -Fe⁴² at 660K and 1428K respectively at which the fcc phase of these two metals are thermodynamically stable. Deviations from the Cauchy relation, as defined by $C_{44} - C_{12}$ are also reported in Table 4. Th appears to be the only fcc metal that obeys the Cauchy equality with $C_{44} \sim C_{12}$ (within 0.2 %), implying that the interatomic forces in Th are largely central. The rest of the fcc metals exhibit substantial deviation from Cauchy equality, implying that non-central and angular forces are operative in the lattices. Furthermore, the deviation for most fcc metals is negative, ie: $C_{44} < C_{12}$, whereas for Ir, γ -Ce, Yb, and δ -Pu-Ga, the deviation is positive, ie. $C_{44} > C_{12}$. The positive deviation appears to associate with variable valency of these elements and/or with the strong electron correlation in these *f* metal systems exemplified by γ -Ce, fcc Pu-Ga, and pure δ -Pu. This point will be discussed further in light of the observed softening of the $T(\xi\xi\xi)$ branch..

Table 4 reports also the anisotropy factor, defined⁴⁴ as the ratio of C_{44}/C' , where $C' = 1/2[C_{11} - C_{12}]$, associated with the two non-degenerate transverse $T_2(\xi\xi0)$ and $T_1(\xi\xi0)$ branches in the phonon dispersion curves shown in Fig. 3. In fcc metals, the elastic anisotropy factor increases from simple p metals like Al to transition metals and rare-earth metals up a value of ~ 4 . For the fcc Pu – 2 at.% Ga alloy, our phonon data shows a high value of 6. The present result confirms an earlier ultrasonic measurement on a higher Ga (3.4 at. %) alloy by Ledbetter and Moment⁴³ who reported a factor of 7

and discussed the elastic properties in δ Pu-Ga alloys in detail. The extremely high elastic anisotropy with regard to propagation of elastic waves in fcc Pu is also substantiated by a recent first principles dynamical mean field theory (DMFT) calculation¹¹ which yielded an even higher theoretical anisotropy factor of 8 for pure δ -Pu.

3. Phonon Density of States, Lattice heat capacity and Debye temperature

Using the phonon dispersion relations derived from the 4NN Born-von Kármán model as shown in Fig. 3, a phonon density of states (DOS) has been computed. The computation was carried out using a grid of $(2\pi/a)/500$, and the result is normalized such that the area under the curve corresponds to 3 states per atom. A Gaussian smoothing by 0.03 meV was applied to produce the final plot shown in Fig. 5(a). The peak at 11.7 meV in the DOS contains major contributions from all three L branches and the $T_2(011)$ branch near the X point. The peak at 6.2 meV has contributions from all branches except the $T(111)$ branch which contributes most significantly to the “rounded-off” feature at 2.1 meV. Critical points obtained from the symmetry points in the zone are indicated in the DOS plot.

The DOS is used to compute the lattice specific heat, c_v , as a function of temperature, and the result is presented in Fig 5(b). At high temperature, c_v approaches the classical Dulong and Petit limit of $3R = 5.96$ cal/mole-K, where R is the molar gas constant. At low temperature, the electronic contribution to the heat capacity, gT , becomes significant.^{45,46} Indeed, by measuring the total heat capacities of a δ -Pu_{0.95}Al_{0.05} alloy and pure α -Pu at low temperatures down to 2K and subtracting the lattice contribution derived from inelastic neutron scattering data⁴⁷, Lashley et al.⁴⁸ found that the g value for the δ phase alloy is almost a factor of 4 higher than that for pure α -Pu, suggesting proximity of the δ phase to a quantum critical point.

From the computed lattice specific heat, the Debye temperature, Θ_D , is also computed as a function of temperature. This is plotted in Fig. 5(c). Above 100K, the Debye temperature, $\Theta_{D(\infty)}$, remains remarkably constant at a value of ~ 119 K. At 0 K, the calculated value $\Theta_{D(0)}$ is 114 K, which is in excellent agreement with the values of 115 K and 120 K determined respectively from ultrasonic measurements⁴³ on a δ Pu-3.4 at. % Ga alloy and from EXAFS measurements⁴⁹ on a δ Pu-1.9 at. % Ga alloy. In Table 5, the Debye temperatures of fcc metals calculated from phonon DOS derived from Born-von Kármán modeling of experimentally determined phonon dispersions are tabulated. It is interesting to note that Au, γ -Fe, and δ Pu-Ga are the only fcc metals with $\Theta_{D(0)} < \Theta_{D(\infty)}$. The increase of Θ_D with Ga content in the δ Pu Ga alloys is merely reflective of the proportional increase in Ga-Pu bonds which have a higher “bond Debye temperature” of 188 K.⁴⁹

4. T(xxx) softening and the $\delta \rightarrow \alpha'$ transformation

The experimental PDCs shown in Fig. 3 display a pronounced softening of the $T[\xi\xi\xi]$ branch towards the L point. A similar feature (but occurring at about twice the energy and at a higher crystal momentum towards the L point) is also seen in a recent dynamic mean field theory (DMFT) calculation of the PDCs of δ -Pu¹¹, (Fig. 6). The softening of this $T[\xi\xi\xi]$ mode is rather unusual in fcc metals, occurring in only two other systems: γ -Ce²⁹ and β -La^{28, 40}, whose PDCs determined by inelastic neutron scattering are reproduced in Fig. 7. The phonon softening in these two systems is temperature dependent, becoming more pronounced at lower temperatures and disappearing at higher temperatures. Based on this evidence, it has been proposed that the observed phonon softening is related to the fcc \rightarrow dhcp phase transformation which occurs in Ce and La at 283K and 660K respectively.²⁹ By analogy, the phonon softening observed in the present experiment on a Pu-Ga alloy may be related to the $\delta \rightarrow \alpha'$ transformation which occurs upon cooling these materials to sub-ambient temperatures.⁵⁰

Measurements of the temperature dependence of the PDCs are being planned in order to validate this hypothesis.

The softening of the $T[\xi\xi\xi]$ branch is also consistent with the crystallography of transformations that occur in γ -Ce, β -La, and δ Pu-Ga alloys. In all cases, the parent phase is the fcc crystal structure which is composed of hexagonal-close-packed atomic planes stacked along the $[111]$ direction with an $ABCABC\dots$ stacking arrangement. The soft transverse mode at L suggests that a (111) plane could be easily sheared relative to its neighboring atomic planes to form new stacking arrangements. In the case of Ce and La the product phase has a dhcp structure with an $ABACABAC\dots$ stacking arrangement, while in the case of Pu-Ga alloys the product phase is a complex monoclinic structure⁵¹ which can also be viewed a distorted hexagonal-close-packed structure with an $ABABAB\dots$ stacking arrangement. It is also possible that the phonon softening is related to the $\delta \rightarrow \gamma$ transformation which occurs in pure Pu and produces a phase with a face-centered orthorhombic structure⁵² which can also be viewed as a stack of slightly distorted hexagonal packed atomic layers which have an $ABABAB\dots$ stacking arrangement. Although this transformation is suppressed in the Pu-Ga alloy studied here, it is possible that the Ga does not completely remove an associated phonon softening. The low energy of the necessary shearing processes involved in these transformations can be seen in the inter-planar force constant of the $T[\xi\xi\xi]$ mode (as derived from the 4NN B-vK model) which is more than an order of magnitude smaller than those of the transverse modes in the other two directions, (see Table 6).

In order to more precisely relate the softening of the $T[\xi\xi\xi]$ branch to the $\delta \rightarrow \alpha'$ transformation in Pu-Ga alloys, we can employ the crystallographic models have been developed by Adler and Olsen⁵³, and more recently by Jin et al.⁵⁴ These models use as a starting point the crystallographic correspondence $(111)_\delta \parallel (020)_\alpha$ and $[-110]_\delta \parallel [100]_\alpha$ which has been established using transmission

electron microscopy by Zocco et al.⁵⁵ Both sets of models predict stable transformation twins with $(205)_\alpha$ twin planes also in agreement with the TEM observations.

In these models, the distortion required to transform a region of the fcc δ phase crystal structure to the monoclinic α' phase crystal structure can be decomposed into three elementary distortions.

- (i). A shuffling operation transforms the fcc structure into an hcp structure by changing the stacking sequence of $\{111\}$ planes
- (ii). A homogeneous elastic strain distorts the hcp structure such that an enlarged 16 atom unit cell has *lattice* vectors which match the *lattice* vectors of the α' phase.
- (iii). A set of periodic displacements modify the *basis* vectors of the distorted, enlarged hcp unit cell such that the α' crystal structure is formed. In this step the *lattice* vectors do not change, only the internal coordinates of the atoms with respect to these vectors. Thus this step does not produce any elastic strain.

The observed phonon softening can be related to the shuffling operation described above. The shuffling operation requires that alternating (111) planes in the fcc lattice be rigidly translated in order to produce the hcp lattice. There are an infinite number of ways in which a shuffling can transform the fcc lattice into the hcp lattice. The simplest mode is a single elementary shuffle and is used in the correspondence suggested Adler and Olsen⁵³ which agrees with the TEM observations.⁵⁵ In this case, every other (111) layer is rigidly shifted by $1/6[-211]$. This shuffling operation is a combination of a zone boundary $T[\xi\xi\xi]$ phonon and a homogeneous shear parallel to the (111) plane. Thus the experimentally observed softening of the $T[\xi\xi\xi]$ phonon is consistent with the proposed model, but we should emphasize that it is only one component of the shuffle operation which itself is only one part of the entire transformation process.

Other more complex shuffling modes are also considered by Jin et al.⁵⁴ They all involve rigidly shifting $\{111\}$ planes to modify the stacking sequence. In these cases, the shuffle includes one or more transverse phonons propagating in the $\langle 111 \rangle$ direction but with different wave-vectors. Again, a homogeneous shear parallel to the $\{111\}$ plane is necessary to complete the shuffle in addition to the appropriate phonon. Each of these proposed shuffle modes lead to different predictions for the habit plane and volume fraction of each twin variant. Further experimental data is needed to clarify which shuffle mode is involved in the phase transformation. In all cases however, a softening of the $T[\xi\xi\xi]$ branch is consistent with the crystallographic models of the $\delta \rightarrow \alpha'$ transformation.

5. The Kohn effect in the $T_1(xx0)$ branch

In Fig. 3 the T_1 branch along $[\xi\xi0]$ exhibits a “kink” with positive dispersion towards the X point, indicative of a Kohn-like anomaly similar to those observed in other fcc metals such as Th³⁵, Au³¹, Pt²⁵ and Pd.³⁰ By analogy with all other phonon anomalies observed in metals, this is likely caused by electronic effects.¹⁹ As the speed of sound of this mode is given by $\sqrt{C'/\rho}$, (ρ = density), it is clear that this anomaly is directly responsible for the small value of C' and implies a soft response of the system to a volume-conserving tetragonal distortion. This may be associated with the high-temperature phase transformation of Pu from δ to δ' (body centered tetragonal) and to ϵ (body centered cubic) which involve just a tetragonal distortion of this type via the so-called Bain path.⁵⁶ Furthermore, these transformations may involve anharmonicity and phonon entropy.¹¹

As mentioned in the introduction, Pu sits in a unique position within the actinide series between elements with itinerant (bonding) and localized (non-bonding) $5f$ electrons^{1,2}. The different polymorphs of Pu have $5f$ electrons that span the range between itinerant and localized behavior. The

exact nature of the $5f$ electrons in Pu is extremely sensitive to changes in intensive parameters such as temperature⁴, pressure⁵⁷ and chemical potential (alloying).⁵⁸ In general, anomalies in PDCs such as those we observe here in δ Pu-Ga are derived from electronic interactions and some of the same anomalies were previously known in other actinide systems. This suggests that the $5f$ electronic structure is the underlying cause for these anomalies. Furthermore, valence instability in the $5f$ electronic structure, together with strong electron-phonon coupling, is likely the underlying reason for both the phonon anomalies we observe as well as the rich variety of polymorphic phase transitions present in this exotic element.

6. Theoretical Considerations

As evident in Fig. 6, the present IXS experiment validates the main qualitative predictions of a recent DMFT calculation by Dai et al. for δ Pu¹¹ in terms of (a) a low shear elastic modulus C' , (b) a Kohn-like anomaly in the $T_1[011]$ branch, and (c) a large softening of the $T[111]$ modes towards L. Such experimental-theoretical agreements give credence to the DMFT approach for the theoretical treatment of $5f$ electron systems of which Pu is a classic example. However, while there is good qualitative agreement between theory and experiment, quantitative differences exist. These are: (i) position of the Kohn anomaly along the $T_1[011]$ branch, (ii) the energy maximum of the $T[111]$ modes and (iii) the softening of the calculated $T[100]$ branch near the X point, which is not observed experimentally in the fcc Pu-Ga alloy.

Dai et al.¹¹ also calculated the phonon dispersion curves for the bcc ϵ -Pu phase with the DMFT method and found that several modes are totally unstable at $T = 0$. Existence of ϵ -Pu at high temperature⁴ was attributed to anharmonicity and final temperature phonon entropy¹¹. On the other hand, the phonon dispersion curves for δ -Pu (Fig. 6) were also computed at $T = 0$. All modes are

found to be stable (no negative frequencies) at all q -values, in spite of the fact that pure δ -Pu is the equilibrium phase only at high temperature in the range 592 - 724 K.⁴

More recently, using a simple inclusion of electron correlations in a Friedel Model of the density of f -electron states, and an empty-core pseudopotential treatment for the three free electrons per atom, Harrison⁵⁹ calculated the phonon dispersion curves of δ -Pu, which contain neither the Kohn effect in the $T_1(110)$ branch nor any softening in the $T(111)$ modes observed experimentally in this study. The derived elastic constants were also in poor agreement with both the earlier ultrasonic work⁴³ and our IXS data. The predicted anisotropy factor was 19 compared with an experimental factor of 6-7 (Table 4).

These differences between the experimental and calculated phonon dispersions are significant and thus provide the framework for refined theoretical treatments¹² and further experiments in Pu and other $5f$ systems.

V. Concluding Remarks

In this paper we have rendered a crystal dynamics analysis of the PDCs of an fcc δ Pu-Ga alloy determined recently⁸ using a *microbeam on large grain sample* experimental concept with high resolution inelastic x-ray scattering to obviate the roadblocks of phonon dispersion measurements on Pu-bearing materials with conventional inelastic neutron scattering. Our results (Fig. 3) represent the first full PDCs ever determined for any Pu-bearing system and end a 40 year quest for this fundamental data for strongly correlated $5f$ systems typified by δ -Pu and its alloys. Our PDC data confirms directly the very high elastic anisotropy of fcc Pu-Ga alloy (highest of all known fcc metals) discovered using ultrasonic measurements⁴³ almost 3 decades ago. More importantly is the pronounced softening observed for the $T[\xi\xi\xi]$ branch. This softening is found to be crystallographically consistent with the meta-stability of the fcc phase of the Pu-Ga alloy and its transformation to a pseudo hexagonal-closed-

pack, monoclinic α' phase via a martensitic transformation. A temperature dependence study of the $T[\xi\xi\xi]$ branch, which is now underway, will hopefully clarify the role of lattice dynamics in the $\delta \rightarrow \alpha'$ transformation in Pu-Ga alloys.

Acknowledgements

This work was performed under the auspices of the U. S. Department of Energy by the University of California, Lawrence Livermore National Laboratory under Contract No. W-7405-Eng-48 and the U.S. Department of Energy by the University of Illinois Frederick Seitz Materials Research Laboratory under Grant No. DEFG02-91ER45439. We are thankful to Francesco Sette for his support and encouragement in this project, and to P. Berkvens and P. Colomp for their advice and technical assistance.

References

* Electronic address: wong10@llnl.gov

1. A. M. Boring and J. L. Smith, Los Alamos Science **26**, 91 (2000).
2. G. Lander, Science, **301** 1057 (2003)
3. R. Jeanloz, Phys. Today **12**, 44 (2000).
4. S. S. Hecker, Los Alamos Science **26**, 290 (2000).
5. S. S. Hecker, Prog. Mater. Science, **49**, 429 (2004).
6. J. T. Orme, M. E. Faiers, B. J. Ward, in the *Proc. of 5th conf, in plutonium an other actinides*, ed. by H. Blank, R. Lindner, New York, North Holland Publishing Co., (1976), p. 761.
7. P. Soderlind and B. Sadigh, Phys. Rev. Lett. **92**, 185702 (2004)
8. Joe Wong, M. Krisch, D. Farber, F. Occelli, A. Schwartz, Tai-C. Chiang, M. Wall, C. Boro and R. Xu, Science, **301**, 1078 (2003).
9. M. E. Manley, G. H. Lander, H. Sinn, A. Alatas, W. L. Hults, R. J. McQueeney, J. L. Smith and J. Willit, Phys. Rev. B **67**, 052302 (2003)
10. S. Y. Savrasov, G. Kotliar, E. Abrahams, Nature, **410**, 793 (2001).
11. X. Dai, S. Y. Savrasov, G. Kotliar, A. Migliori, H. Ledletter, and E. Abrahams, *Science* **300**, 953 (2003).
12. G. Kotliar and D. Vollhardt, Phys. Today, **57**, 53 (2004)
13. J. C. Lashley, M. G. Stout, R. A. Pereyra, M.S. Blau, J. D. Embury, Scripta Mater. **44**, 2815 (2001).
14. W. H. McMaster, N. Nerr del Grande, J. H. Mallett, and J. H. Hubbel, Lawrence Radiation Laboratory Report No. UCRL-50/74 sec. 2 Rev., (1969).
15. ESRF Procedures for experiments using radioactive samples on beam lines other than BM20.
16. F. Occelli, M. Krisch, P. Loubeyre, F. Sette, R. Le Toullec, C. Masciovecchio, and J.-P. Rueff, Phys. Rev. B **63**, 4306 (2001).
17. M. D'Astuto, P. K. Mang, P. Giura, A. Shukla, P. Ghigna, A. Mirone, M. Braden, M. Greven, M. Krisch and F. Sette, Phys. Rev. Lett. **88**, 167002 (2002); H. Requardt, J. E. Lorenzo, P. Monceau, R. Currat, M. Krisch, Phys. Rev. B **66**, 214303 (2002).
18. M. Born, K. Huang, *Dynamical Theory of Crystal Lattices*. (Clarendon Press, Oxford, England, 1954).
19. W. Kohn, Phys. Rev. Lett. **2**, 393 (1959).
20. E. C. Svensson, B. N. Brockhouse and J. W. Rowe, Phys. Rev., **155**, 619 (1967).
21. D. H. Dutton and B. N. Brockhouse and A. P. Müller, Can. J. Phys. **50**, 2915 (1972).
22. Ref. 18, p. 142
23. C. Kittel, *Introduction to Solid State Physics*, 3rd Ed., John Wiley, New York (1967), p. 122

24. R. E. MacFarlane, J. A. Rayne and C. K. Jones, Phys. Lett. **20**, 234 (1966)
25. R. E. Macfarlane, Phys. Lett. **18**, 91 (1965)
26. E. Walker, J. Ashkenazi and M. Dacorogna, Phys. Rev. B, **24**, 2254 (1981)
27. R. J. Birgeneau, J. Cordes, G. Dolling and A. D. B. Woods, Phys. Rev. **136**, A1359 (1964)
28. C. Stassis, G. S. Smith, B.N. Harmon, K.-M. Ho and Y. Chen,, Phys. Rev. B **31**, 6298 (1985).
29. C. Stassis, T. Gould, O. D. McMasters, K. A. Gschneidner Jr., R. M. Nicklow, *Phys. Rev. B* **19**, 5746 (1979); C. Stassis, C.-K. Loong, O.D. McMasters, R. M. Nicklow, *Phys. Rev. B* **25**, 6485 (1982).
30. J. A. Rayne, Phys. Rev. **118**, 1545 (1960)
31. J. W. Lynn, H. G. Smith and R. M. Nicklow, Phys. Rev. B **8**, 3493 (1973).
32. W. Drexel, Z. Phys. **205**, 281 (1972).
33. W. C. Overton, Jr., J. Gaffney, Phys. Rev. **98**, 969 (1955)
34. C. Stassis, J. Zarestky, D. K. Misemer, H. L. Skriver, and B. N. Harmon, Phys. Rev. B **27**, 3303 (1983).
35. P. E. Armstrong, O. N. Carlason and J. F. Smith, J. Appl. Phys. **30**, 36 (1959).
36. R. A. Reese, S. K., Sinha and D. T. Peterson, Phys. Rev. B **8**, 1332 (1973)
37. U. Buchenau, M. Heiroth, H. R. Schober, J. Evers and G. Oehlinger, Phys. Rev. B **30**, 3502 (1984)
38. D. L. Waldorf, Bull. Am. Phys. Soc. **5**, 170 (1960).
39. B. N. Brockhouse, T. Arase, G. Caglioti, K. Rao, and A. D. Woods, Phys. Rev. **128**, 1099 (1962).
40. C. Stassis, C.-K. Loong, J. Zarestky, Phys. Rev. B **26**, 5426 (1982).
41. C. Stassis, C.-K. Loong, and C. Theisen, Phys. Rev. B **26**, 4106 (1982)
42. J. Zarestky and C. stasis, Phys. Rev. B **35**, 4500 (1987).
43. H. M. Ledbetter, R.L. Moment, Acta Metallurgica **24**, 891 (1976).
44. C. Zener, *Elasticity and Anelasticity of Metal*,. Univ. Chicago Press. Chicago, IL (1948), p. 16
45. A. P. Miiller and B.N. Brockhouse, Can. J. Phys. **49**, 704 (1971).
46. A. P. Miiller and B.N. Brockhouse, Phys. Rev. Lett, **20** 798 (1968).
47. R. J. McQueeney, A. C. Lawson, A. Migliori, T. M. Kelley, B. Fultz, M. Ramos, B. Martinez, J. C. Lashley, and Sven C. Vogel, Phys. Rev. Lett. **92**, 146401 (2004)
48. J. C. Lashley, J. Singleton, A. Migliori, J. B. Betts, R. A . Fisher, J. L. Smith and R. J. McQueeney, Phys. Rev. Lett. **91**, 205901 (2003).
49. E. J. Nelson, K. J .M. Blobaum, M. A. Wall, P. G. Allen, A. J. Schwartz and C. H. Booth, Phys. Rev. B **67**, 224206 (2003).
50. S. S. Hecker, L. F. Timofeeva, *Los Alamos Sci*, **26**, 244 (2000)
51. W. H. Zachariasen, F. H. Ellinger, Acta Cryst. **16**, 777 (1963).

52. W. H. Zachariasen, F. H. Ellinger, *Acta Cryst.* **8**, 431 (1955)
53. P. H. Alder, G. B. Olson, and D. S. Margolies, *Acta Metall.* **34**, 2053 (1986)
54. Y. M. Jin, Y. U. Wang, A. G. Khachaturyan, C. R. Krenn, A. J. Schwartz, *Metall. Mater. Trans. A.* (2004) submitted
55. T. G. Zocco, M. F. Stevens, P. H. Alder, R. T. Sheldon and G. B. Olson, *Acta Metall. Mater.* **38**, 2275 (1990).
56. R. W. K. Honeycombe, *Steels: Microstructure and Properties*, Edward Arnold Publ. London (1980), p. 81
57. S. Heathman, R. G. Haire, T. Le Bihan, a. Lindbaum, K. Litfin, Y. Meresse, and H. Libotte, *Phys. Rev. Lett.* **85**, 2961 (2000).
58. A. Gschneidner, Jr., R. O. Elliot, R. R. McDonald, *J. Phys. Chem* **23**, 1191 (1962).
59. W. A. Harrison, *Phys. Rev. B* **69**, 113106 (2004).

Figure Captions

Figure 1. Optical micrograph showing the large-grain microstructure of the fcc Pu-Ga 2 at. % alloy used in this study. The white box denotes the footprint on the sample of a $30\text{ }\mu\text{m} \times 60\text{ }\mu\text{m}$ x-ray beam used to collect the HRIXS phonon spectra.

Figure 2. Representative inelastic x-ray scattering spectra for the longitudinal acoustic phonon branch along the $[111]$ direction in a δ Pu-2 at. % Ga alloy. The experimental data (points) are shown together with the results of the best fit model (lines) of the phonon and elastic contributions. In each panel, the reduced phonon wave vectors, ξ , is indicated to the left of the spectra and the phonon energy to the right.

Figure 3. The phonon dispersion curves of a δ fcc Pu-2 at. % Ga alloy at room temperature. The longitudinal and transverse modes are denoted L and T respectively. The circles represent the experimental points. The transverse branches along each of the $[\xi 00]$ and $[\xi \xi \xi]$ directions are degenerate. Along the $[\xi \xi 0]$ direction, the two transverse branches are distinct: $T_1[011]$ polarized along $\langle 01\bar{1} \rangle$ and $T_2[011]$ polarized along $\langle 001 \rangle$. Note the softening of the $TA[\xi \xi \xi]$ branch towards the L point. The solid curves represent a fourth-nearest neighbor (4NN) Born-von Kármán model fit to the experimental data. The lattice parameter of our samples is $a = 0.4621\text{ nm}$.

Figure 4. A statistical estimate of the goodness of fit χ^2 for a Born-von Kármán model plotted as a function of the number of nearest neighbors included in the model.

Figure 5. (a) The density of states (DOS), (b) lattice specific heat and (c) Debye temperature of an fcc Pu-2 at. % Ga alloy calculated from a 4NN Born-von-Kármán model. Critical points in the DOS obtained from the symmetry points in the zone are indicated in (a).

Figure 6. Comparison of calculated phonon dispersions (lines) for pure δ Pu using DMFT-linear response theory by Dai et al.¹¹ with the present experimental dispersions (circles) for an fcc δ Pu-Ga alloy, showing overall qualitative agreement.

Figure 7. Room temperature phonon dispersion curves of (a) fcc γ -Ce²⁹ and (b) fcc β -La²⁸, showing softening of the $T[\xi \xi \xi]$ branch observed similarly in the current Pu-Ga alloy. In each case, the smooth curves represent a 8NN Born-von Kármán force-constant model fit to the inelastic neutron scattering data. (Reproduced with permission from the authors).

Table 1. Normal mode phonon energies for the symmetry branches in a d Pu- 2 at.% Ga alloy at room temperature.

L (0, 0, x)		T (0, 0, x)	
<u>x</u>	<u>meV</u>	<u>x</u>	<u>meV</u>
0	0	0	0
0.185	2.38 ± 0.3	0.15	1.93 ± 0.1
0.296	4.23 ± 0.2	0.2	2.52 ± 0.1
0.407	6.0 ± 0.2	0.3	3.82 ± 0.15
0.506	7.45 ± 0.2	0.4	4.79 ± 0.13
0.619	8.85 ± 0.3	0.6	6.17 ± 0.082
0.729	10.4 ± 0.2	0.75	6.72 ± 0.07
0.838	11.8 ± 0.2	0.9	6.93 ± 0.08
0.951	12.6 ± 0.3	1	6.92 ± 0.09
0.941	12.21 ± 0.4		

L (0, x, x)		T₂ (0, x, x)	
<u>x</u>	<u>meV</u>	<u>x</u>	<u>meV</u>
0	0	0	0
0.1	2.42 ± 0.06	0.2	3.57 ± 0.1
0.2	4.63 ± 0.12	0.4	6.89 ± 0.15
0.25	6.13 ± 0.14	0.6	9.75 ± 0.25
0.35	8.53 ± 0.3	0.8	12.34 ± 0.4
0.4	9.23 ± 0.11		
0.51	10.28 ± 0.3		
0.56	10.37 ± 0.4		
0.66	10.65 ± 0.2		
0.72	9.72 ± 0.4		
0.81	8.54 ± 0.4		

L (x, x, x)		T₁ (0, x, x)	
<u>x</u>	<u>meV</u>	<u>x</u>	<u>meV</u>
0	0	0	0
0.072	2.27 ± 0.1	0.2	1.45 ± 0.05
0.1	3.11 ± 0.12	0.3	2.14 ± 0.06
0.15	4.93 ± 0.28	0.45	3.56 ± 0.1
0.2	6.41 ± 0.15	0.5	3.9 ± 0.1
0.23	7.45 ± 0.15	0.6	5.01 ± 0.15
0.28	9.02 ± 0.3	0.7	5.43 ± 0.3
0.32	10.27 ± 0.2	0.85	6.49 ± 0.3
0.35	10.9 ± 0.2		
0.4	11.91 ± 0.3		
0.43	12.1 ± 0.4		
0.45	12.6 ± 0.3		
0.47	12.8 ± 0.3		
0.48	12.8 ± 0.3		

T (x, x, x)	
<u>x</u>	<u>meV</u>
0	0
0.075	1.22 ± 0.1
0.1	1.52 ± 0.07
0.15	2.164 ± 0.06
0.2	2.56 ± 0.06
0.3	2.83 ± 0.06
0.4	2.34 ± 0.06
0.5	1.98 ± 0.06

Table 2. Born von-Karman atomic force constants, (Nm⁻¹)

Constraints for 8NN and 7NN: $8(5ZZ)=9(5YY) - 5XX$; $8(5XY)=3(5XX - 5YY)$; $3(7YZ)=7XY$; $2(7XZ)=7XY$

Constraints for 6NN and 5NN: $8(5XY)=3(5XX - 5YY)$

No constraints for 4NN, 3NN and 2NN.

	2NN	3NN	4NN	5NN	6NN	7NN	8NN
1XX	8.305	8.1149	9.4001	9.3616	9.2694	9.145	9.0172
1ZZ	-2.081	-0.7228	-2.1735	-2.2841	-2.3653	-2.5584	-2.1621
1XY	8.557	11.3954	11.296	11.2949	11.2981	11.4838	11.5481
2XX	-1.929	-0.7896	-3.0938	-2.9988	-3.0892	-2.9408	-2.8591
2YY	-0.707	-0.1357	0.9046	0.9719	1.1133	1.2634	0.6954
3XX		-1.3769	-0.5516	-0.4387	-0.3527	-0.4641	-0.7061
3YY		0.4561	-0.2943	-0.2915	-0.2499	-0.0928	-0.1324
3YZ		-0.587	-0.4259	-0.4245	-0.4224	-0.438	-0.5226
3XZ		-0.5389	-0.3239	-0.3074	-0.3014	-0.3401	-0.2841
4XX			-0.0657	-0.0284	-0.0586	-0.1854	-0.0202
4ZZ			0.9747	0.974	0.9729	1.0115	0.7709
4XY			-0.4969	-0.538	-0.5856	-0.6857	-0.8681
5XX				-0.084	-0.0582	0.0141	0.3726
5YY				-0.0369	-0.0141	-0.1258	0.0303
5ZZ				-0.0015	-0.0694	-0.1433	-0.0125
5XY				-0.0176	-0.0165	0.0525	0.1284
6XX					-0.0698	-0.1863	-0.031
6YZ					0.0255	0.0966	0.218
7XX						0.0003	0.0425
7YY						0.1319	-0.0184
7ZZ						-0.048	-0.0279
7YZ						-0.0056	-0.0186
7XZ						-0.0084	-0.0279
7XY						-0.0168	-0.0557
8XX							-0.9241
8YY							0.0101
C²	2010.8	67.8	35.6	33.7	27.7	21.1	14.1

Table 3. Sound velocities v (ms^{-1}), and elastic moduli, C_{ij} for δ Pu-2 at. % Ga (GPa). The elastic moduli for both a Pu-3.4 at. % Ga alloy by ultrasonics and pure δ Pu calculated using DMFT are also listed for comparison

$V_{100} \text{ L} = 1586 \pm 20$	$V_{110} \text{ L} = 1894 \pm 20$	$V_{111} \text{ L} = 2080 \pm 30$
$V_{100} \text{ T} = 1379 \pm 30$	$V_{110} \text{ T}_1 = 566 \pm 4$	$V_{111} \text{ T} = 979 \pm 45$
	$V_{110} \text{ T}_2 = 1411 \pm 16$	

System	C_{11}	C_{12}	C_{44}	Remarks
δ Pu-2 at. % Ga	35.3 ± 1.4	25.5 ± 1.5	30.53 ± 1.1	This work
δ Pu-3.4 at. % Ga	36.28	26.73	33.59	Ultrasonics ⁴³
δ Pu	34.56	26.81	33.03	DMFT ¹¹

Table 4. Elastic constants C_{ij} of fcc metals (in units of GPa) at 300K - Cauchy inequality: $C_{44} - C_{12}$, and anisotropy factor: $C_{44}/1/2[C_{11} - C_{12}]$. Except for Rh, Ir, Pt, Th and Pu-Ga, all elastic moduli were determined from inelastic neutron scattering measurements.

Metal	C_{11}	C_{12}	C_{44}	Cauchy inequality $C_{44} - C_{12}$	Anisotropy factor $2C_{44}/[C_{11} - C_{12}]$	Ref.
Al	106.8	60.7	28.2	- 32.5	1.223	23
Ir (ultrasonic)	600	260	270	+10	1.588	24
Pt (90K) (ultrasonic)	346.7	250.7	76.5	-174.2	1.594	25
Rh (ultrasonic)	413	194	184	-10	1.680	26
Ni	250.8	150.0	123.5	- 26.5	2.450	27
β -La (300K)	34.47	20.38	17.96	- 2.42	2.549	28
γ -Ce	24.1	10.2	19.4	+ 9.2	2.79	29
Pd	227.1	176.1	71.7	- 104.4	2.811	30
Au	192.3	163.1	42.0	- 121.1	2.876	31
Ag	124.0	93.7	46.1	- 47.6	3.042	32
Cu	168.4	121.4	75.4	- 46.0	3.208	33
Ca	27.8	18.2	16.3	- 1.9	3.396	34
Th (ultrasonic)	75.3	48.9	47.8	- 0.11	3.621	35, 36
Sr	15.3	10.3	9.9	-0.4	3.960	37
Pb	49.5	42.3	14.9	- 27.4	4.138	38, 39
β -La (660K)	28.46	20.41	16.53	- 3.88	4.106	40
Yb	18.6	10.3	17.7	+ 7.4	4.265	41
γ -Fe (1428K)	154	122	77	-45	4.813	42
δ Pu-Ga (IXS) [2 at. % Ga]	35.30	25.5	30.53	+ 5.03	6.059	This work
δ Pu-Ga (ultra) [3.4 at. % Ga]	36.28	26.73	33.59	+6.86	7.03	43

Table 5. Calculated Debye temperatures Θ_D of fcc metals from DOS derived from B-vK modeling of experimental phonon dispersions

Metal	Θ_0 (K)	Θ_∞ (K)	$\Theta_0 > \Theta_\infty$^(a)	B-vK Model^(b)	Ref.
Ni	450	385	Y	5NN	27
Al	410	395	Y	8NN	23
Cu	333	313	Y	6NN	33
γ -Fe	324	330	N	6NN	42
Ag	223	215	Y	4NN	32
Ca	216	213	Y	8NN	34
Pd	- ^(c)	275			30
Pt (90K)	- ^(c)	230			25
Au	159	183	N	4NN	31
Th	158	142	Y	7NN	35
β -La (300K)	139	122	Y	8NN	28
γ -Ce $4f^1 5d^1 6s^2$	135	119	Y	8NN	29
β -La (660K)	134	123	Y	8NN	40
Yb $4f^{14} 5d^0 6s^2$	109	105	Y	2NN	41
Pb	- ^(c)	88		>8NN	38
δ Pu-Ga $5f^6 6d^1 7s^2$ (2 at. %)	114	119	N	4NN	This work
δ Pu-Ga (1.9 at. %)	120 ^(d)	- ^(c)		EXAFS	49
δ Pu-Ga (3.4 at. %)	115	- ^(c)		ultrasonics	43
δ Pu-Ga (6.8 at. %)	127	- ^(c)		ultrasonics	43
δ Pu-Ga (10.2 at. %)	133	- ^(c)		ultrasonics	43

(a) Θ_0, Θ_∞ = Debye temperatures at 0 K and ∞ K respectively. For all fcc metals listed above, $\Theta_0 > \Theta_\infty$, except for γ -Fe, Au, δ Pu-Ga.

(b) NN = nearest neighbors. 8NN means that interactions up to 8 nearest neighbor have been taken into account for a good fit of the PDC data with the B-vK model.

(c) Not calculated

(d) Derived from the Pu-Pu bond correlation. The corresponding Debye temperature from the Ga-Pu correlation is 188K.

Table 6. Interplanar force constants (Nm^{-1}) for d Pu-2 at. % Ga calculated from the 4NN B-vK model

Branch	F_1	F_2	F_3	F_4
[00 ξ] L	70.552	-11.138		
[00 ξ] T	22.156	3.09		
[0 $\xi\xi$] L	28.136	37.802	-5.98	-1.128
[0 $\xi\xi$] T ₂	72.912	-3.468	-2.36	1.952
[0 $\xi\xi$] T ₁	22.95	-4.014	-0.796	0.864
[$\xi\xi\xi$] L	74.774	-6.884		
[$\xi\xi\xi$] T	1.826	2.548		

Fig. 1

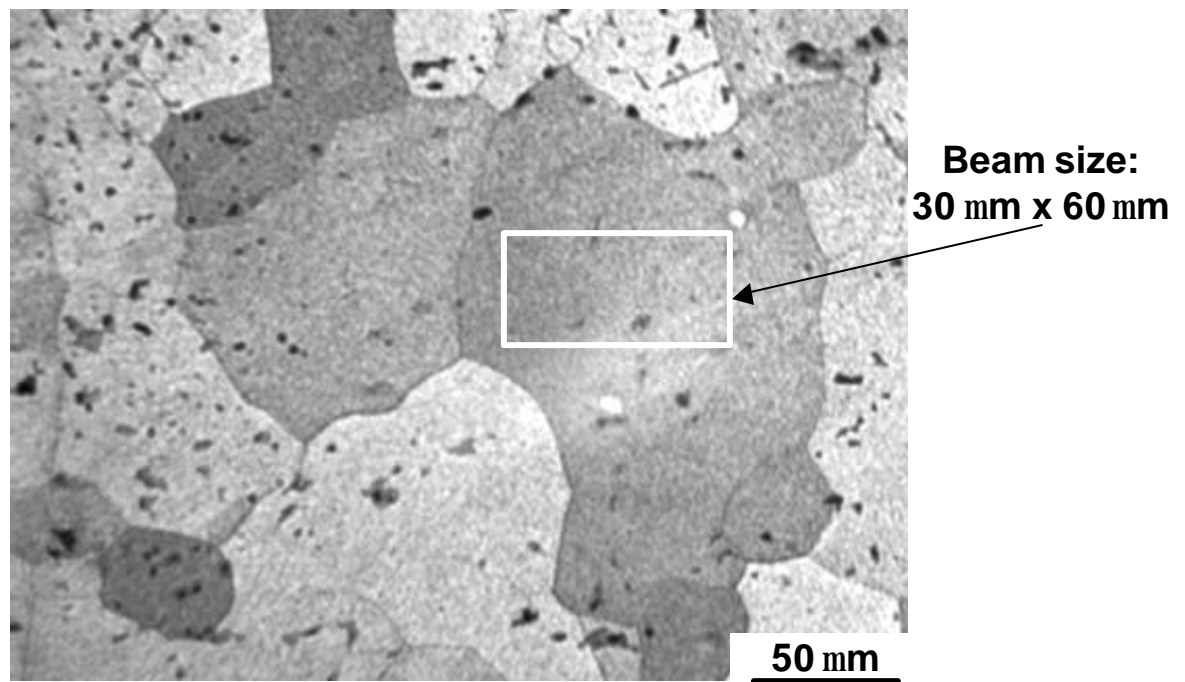


Fig. 2

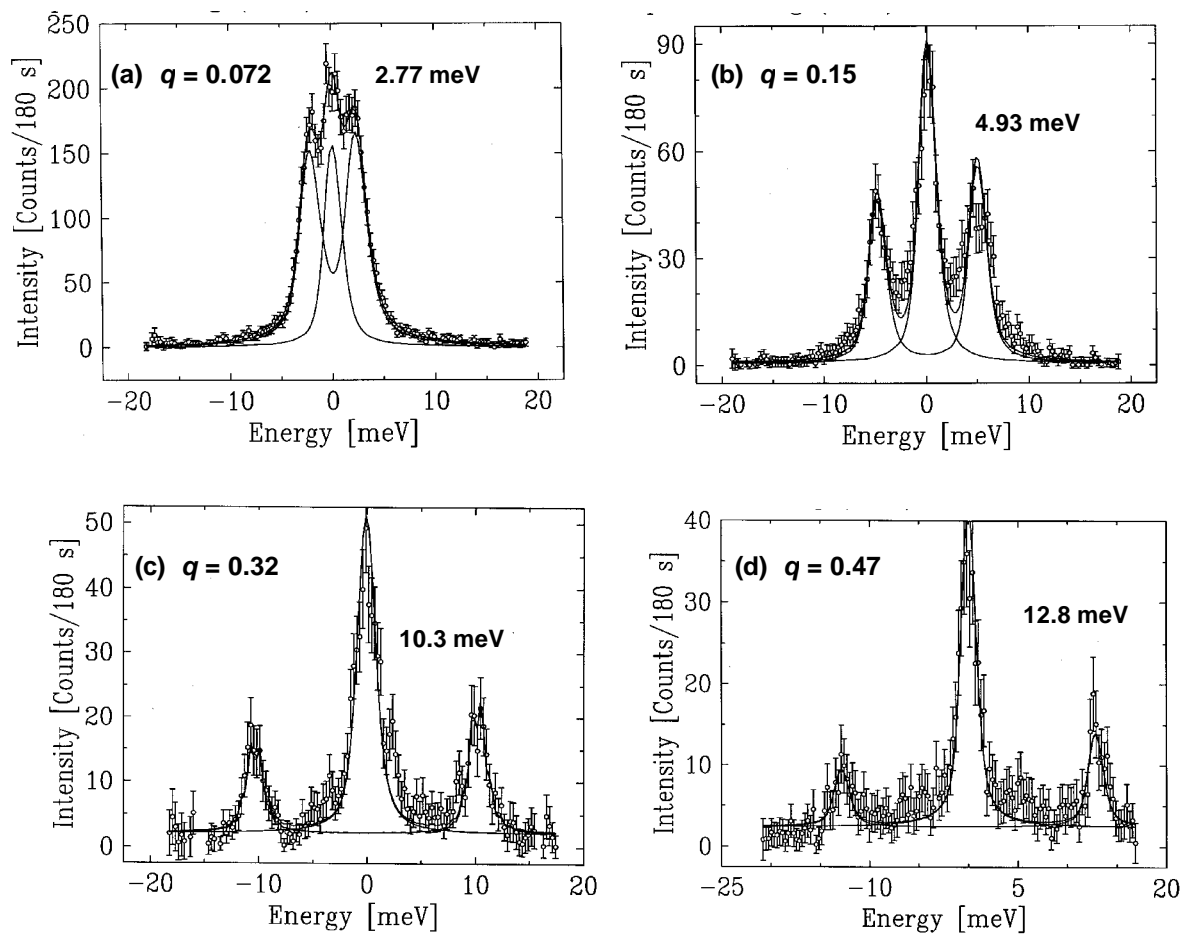


Fig 3

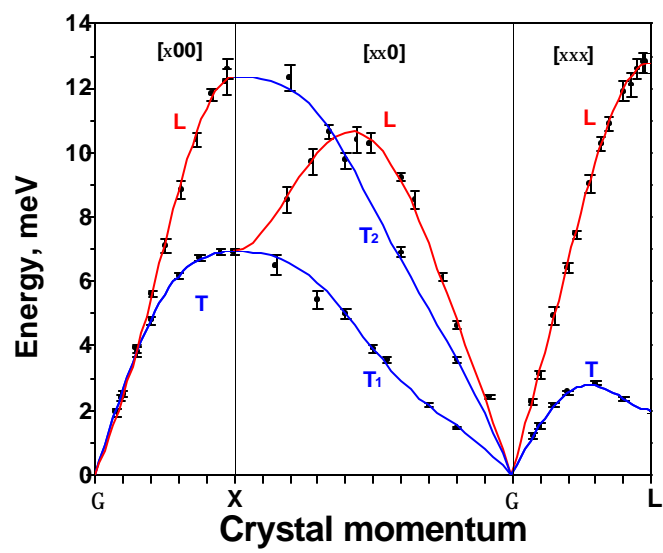


Fig. 4

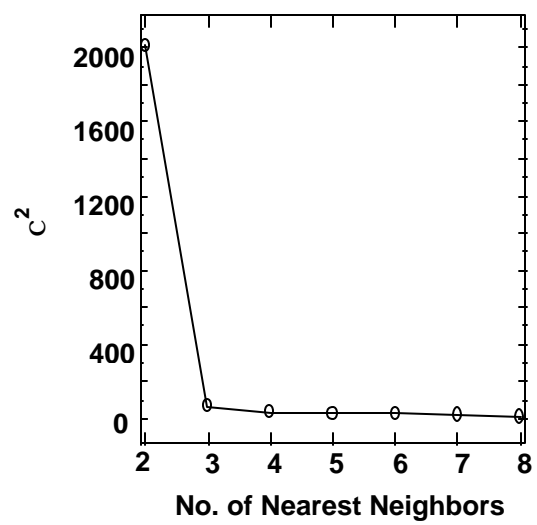


Fig. 5

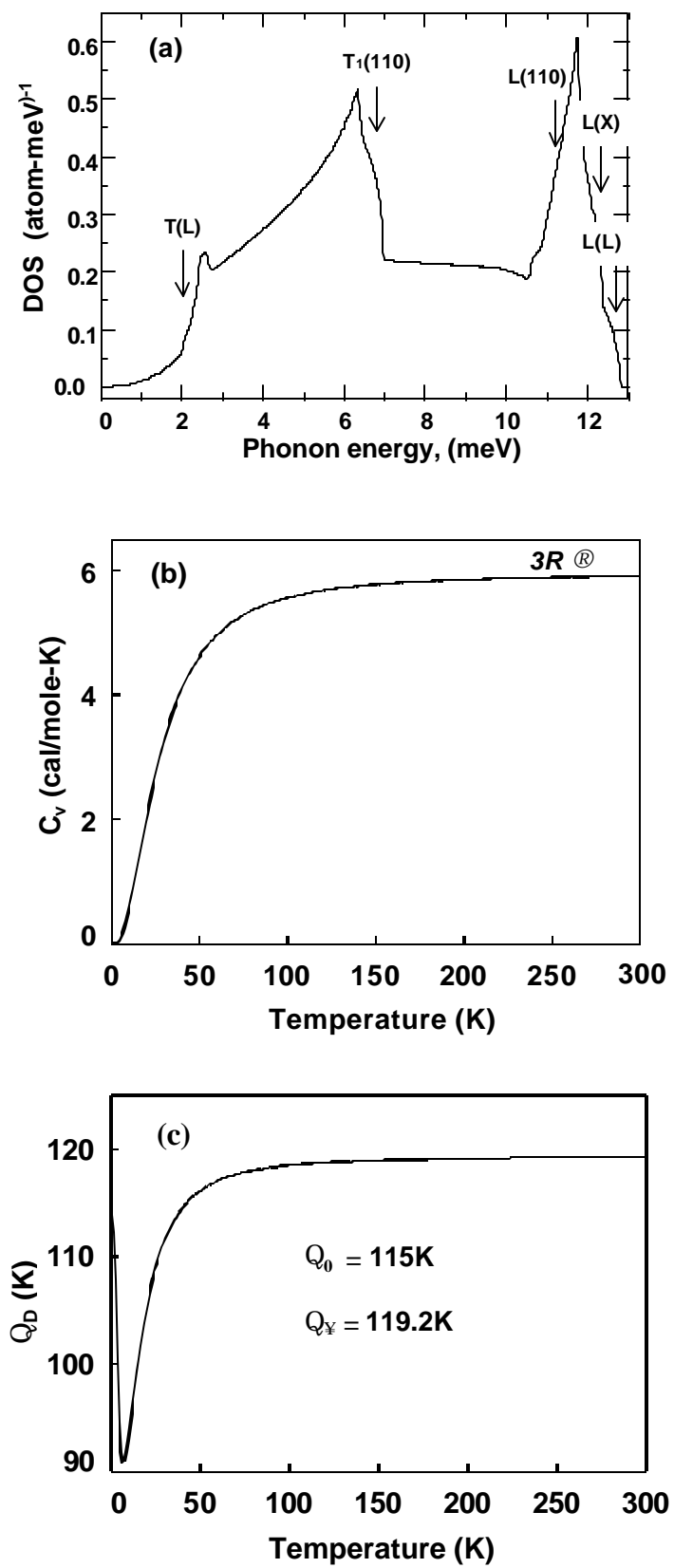


Fig. 6

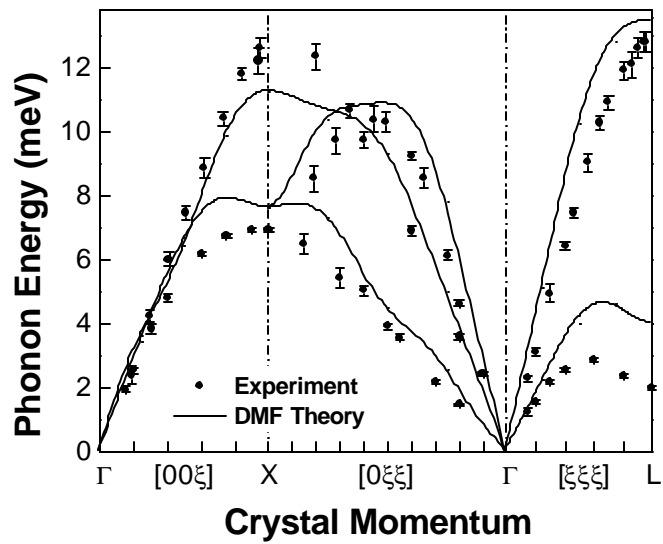
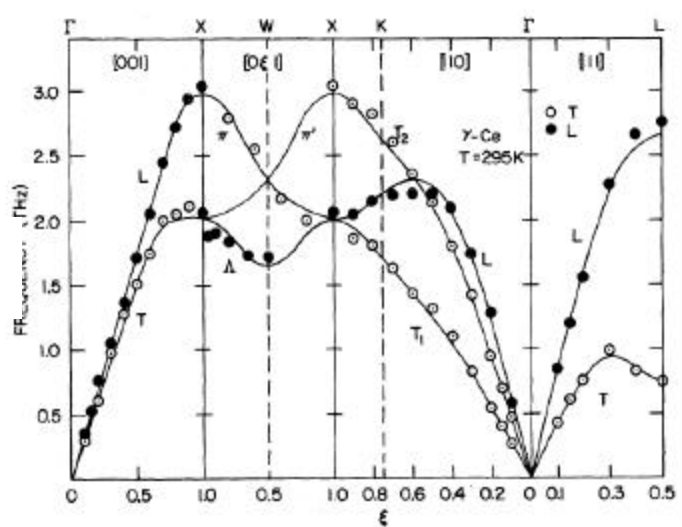


Fig. 7

(a)



(b)

